

# Ménec Fossae on Europa: A Strike-Slip Tectonics Origin above a possible Shallow Water Reservoir

Pietro Matteoni<sup>1</sup>, Alicia Neesemann<sup>2</sup>, Ralf Jaumann<sup>3</sup>, Jon K. Hillier<sup>4</sup>, and Frank Postberg<sup>5</sup>

<sup>1</sup>Planetary Sciences and Remote Sensing, Institute of Geological Sciences, Freie Universität Berlin

<sup>2</sup>Freie Universität Berlin Fachbereich Geowissenschaften

<sup>3</sup>Freie Universität Berlin Institut für Geologische Wissenschaften

<sup>4</sup>Institute of Geological Sciences, Freie Universität Berlin

<sup>5</sup>Freie Universitaet Berlin

November 21, 2022

## Abstract

Faults and fractures may emplace fresh material onto Europa's surface, originating from shallow reservoirs within the ice shell or directly from the subsurface ocean. Ménec Fossae is a region of particular interest, as it displays, within a relatively small area, the interaction of several geological features such as bands, double ridges, chaotic terrains, and fossae. These features might affect the emplacement of buried material and subsequent exposure of fresh volatiles, prime targets for the upcoming JUICE and Europa Clipper missions in order to assess Europa's astrobiological potential. Previous studies already revealed that a deep central trough is present at Ménec Fossae, flanked by several subparallel minor troughs and by few asymmetrical scarps with lobate planforms. The presence of such features has motivated this study, given its potential to provide clear indications on the tectonic regime involved. Through detailed geomorphological-structural mapping on Galileo Solid State Imager data and terrain analysis on Digital Terrain Models, we could develop a novel hypothesis on the formation mechanisms that might have been involved in the study area. We propose that Ménec Fossae has been shaped by transtensional (strike-slip with a major extensional component) tectonic activity, as indicated by the orientation and relationship of the tectonic features present. The shear heating related to such a tectonic setting possibly led to the formation of a shallow water reservoir, that in turn could have generated the observed chaotic terrains, double ridges, and fossae. These results strengthen the case for widely distributed shallow water reservoirs within Europa's ice shell.



## 18 **Abstract**

19 Faults and fractures may emplace fresh material onto Europa's surface, originating from shallow  
20 reservoirs within the ice shell or directly from the subsurface ocean. Méneç Fossae is a region of  
21 particular interest, as it displays, within a relatively small area, the interaction of several  
22 geological features such as bands, double ridges, chaotic terrains, and fossae. These features  
23 might affect the emplacement of buried material and subsequent exposure of fresh volatiles,  
24 prime targets for the upcoming *JUICE* and *Europa Clipper* missions in order to assess Europa's  
25 astrobiological potential. Previous studies already revealed that a deep central trough is present at  
26 Méneç Fossae, flanked by several subparallel minor troughs and by few asymmetrical scarps  
27 with lobate planforms. The presence of such features has motivated this study, given its potential  
28 to provide clear indications on the tectonic regime involved. Through detailed  
29 geomorphological-structural mapping on *Galileo* Solid State Imager data and terrain analysis on  
30 Digital Terrain Models, we could develop a novel hypothesis on the formation mechanisms that  
31 might have been involved in the study area. We propose that Méneç Fossae has been shaped by  
32 transtensional (strike-slip with a major extensional component) tectonic activity, as indicated by  
33 the orientation and relationship of the tectonic features present. The shear heating related to such  
34 a tectonic setting possibly led to the formation of a shallow water reservoir, that in turn could  
35 have generated the observed chaotic terrains, double ridges, and fossae. These results strengthen  
36 the case for widely distributed shallow water reservoirs within Europa's ice shell.

37

## 38 **Plain Language Summary**

39 Tectonic cracks may emplace fresh material onto Europa's surface, that can originate from  
40 shallow water bodies within the icy crust or directly from the subsurface ocean. This kind of  
41 material is a prime target for upcoming space missions in order to assess Europa's habitability.  
42 We investigated the area of Méneç Fossae, which is characterized by many different geological  
43 features and structures within a relatively small area and can therefore provide clues on the  
44 mechanisms that shaped it. Our analysis were based on imaging and new topographic data, we  
45 developed a new hypothesis involving a combination of different tectonic styles as the driving  
46 processes for the formation of this area. This kind of tectonic activity could be related to heating  
47 through shear friction, which might have generated a liquid water pocket at shallow depths  
48 within Europa's icy crust, explaining the concurrent presence of some particular geological  
49 features. These findings strengthen the case for shallow water pockets to be widely distributed  
50 within the icy crust, which could allow future space missions to more easily assess Europa's  
51 habitability.

52

## 53 **1 Introduction**

54 Amongst the three possible Jovian ocean worlds, Europa, Ganymede and Callisto, the  
55 most detailed and convincing evidence for an internal ocean has been obtained for Europa (e.g.,  
56 Nimmo & Pappalardo, 2016). Not only does the magnetic induction response to Jupiter's time-  
57 varying magnetic field indicate the existence of a subsurface salty ocean (Khurana et al., 1998;  
58 Kivelson et al., 2000), but the moon's surface also shows indications of interaction with a liquid  
59 layer beneath the ice crust. Images from Voyager 2 and Galileo show a fractured icy surface,  
60 with regions where ice crust blocks seem to have moved in a slushy or liquid medium (Carr et

61 al., 1998; Pappalardo et al., 1999). The orientation of some large-scale linear features also seems  
62 to have changed over time, implying rotation of the ice shell and a very low viscosity layer  
63 between the interior and the surface (Pappalardo et al., 1998). The thickness and thermo-physical  
64 structure of the ice shell are poorly constrained, but models suggest it may be 20–30 km thick  
65 (e.g., Howell, 2021; Hussmann, 2002; Quick & Marsh, 2015), with a layer of warm, convecting  
66 ice underlying a cold, rigid crust (Barr & Pappalardo, 2005; Pappalardo et al., 1998).

67 Pressures at the base of the internal global ocean are too low for the formation of high-  
68 pressure ice phases, and the ocean is thus believed to be in contact with the rocky interior  
69 (Anderson et al., 1998). This raises the possibility of rich chemical exchange between the silicate  
70 interior and the subsurface ocean, perhaps via hydrothermal vents, and potentially chemical  
71 heating through serpentinization (Vance et al., 2007; Vance et al., 2016). Since long-lived  
72 radioactive elements are expected to be present in the silicates, as they are within the Earth, a  
73 further source of energy that heats the rocky interior is radioactive decay (Běhounková et al.,  
74 2021; Hussmann et al., 2010). However, the major heating source is provided by tidal dissipation  
75 due to Europa's eccentric orbit, maintained over long time periods by orbital resonances with Io  
76 and Ganymede (Schubert et al., 2009; Sotin et al., 2009). These considerations make Europa one  
77 of the main candidates in the Solar System for supporting the development of life (Greenberg et  
78 al., 2000; Greenberg & Geissler, 2002). If biosignatures are produced within Europa's ocean,  
79 they will need to reach the surface to be detected by the upcoming Jupiter Icy Moons Explorer  
80 (*JUICE*) and *Europa Clipper* missions. There are indications of salts at some surface locations  
81 (e.g., Dalton et al., 2005; Trumbo et al., 2019), consistent with recent extrusions or ejections of  
82 salt-rich liquid water from the moon's interior. Some investigators have recently suggested that  
83 the salt minerals present on Europa's surface may be dominated by endogenic chlorinated  
84 species (e.g., sodium and/or magnesium chlorides), rather than by sulfates (Hand & Carlson,  
85 2015; Ligier et al., 2016; Trumbo et al., 2017, 2019a, 2019b, 2022), which were the main  
86 previously hypothesized compounds (e.g., Dalton et al., 2012; Hansen & McCord, 2008;  
87 McCord et al., 1999; Orlando et al., 2005), with radiolysis producing the observed reddish-brown  
88 coloration of *lineae* and *chaos* regions. A chloride-rich, sulfate-poor ocean would likely be  
89 indicative of ongoing water/rock interaction at the seafloor, whereas a sulfate-rich, chloride-poor  
90 ocean could indicate either a primordial, leached composition or significant cycling with the ice  
91 shell and delivery into the ocean of radiolytically-produced sulfates (Hand et al., 2022).

92 At global scales, landform evolution on atmosphereless bodies is primarily driven by  
93 impact gardening, tectonics, and (cryo-)volcanism. Crater density and frequency analysis  
94 indicate that Europa's geologically active surface (Greenberg et al., 1998; Greenberg & Geissler,  
95 2002) is relatively young (~40-90 My, Bierhaus et al., 2009), with a wide variety of landforms  
96 including ridges, troughs, bands, lenticulae, and chaotic terrains (Greeley et al., 2004; Greeley et  
97 al., 2000). To understand which resurfacing processes are responsible for Europa's anomalously  
98 young surface age, several compressional mechanisms have been invoked, such as subduction  
99 (cold, brittle, and dense outer portions of the ice shell sink into the underlying convecting  
100 warmer ice, in analogy to Earth's convergent plate boundaries; Kattenhorn & Prockter, 2014)  
101 and regional scale folding (e.g., Prockter & Pappalardo, 2000). Nevertheless, the tectonic regime  
102 that dominates within the ice shell is extensional, a hypothesis supported by numerous lines of  
103 evidence, such as the widespread presence of dilational bands that represent >40% of the total  
104 surface area (Kattenhorn & Hurford, 2009). Several types of geological features generated within  
105 such a tectonic regime, including bands, double ridges, cycloids, chaotic terrains, and fossae,

106 might affect the emplacement of buried material and subsequent exposure of fresh volatiles on  
107 Europa's surface.

108 Bands (Figure 1a), on Europa, are tabular zones of dilation in the icy shell where new  
109 crustal material intruded between the walls of a crack (Kattenhorn & Hurford, 2009); they have  
110 lengths of hundreds of km and widths of a few km up to ~30 km. Bands are thought to represent  
111 a phenomenon analogous to Earth's mid-ocean ridge spreading centers, potentially making them  
112 the only other known feature in the Solar System where complete lithospheric separation has  
113 occurred (Kattenhorn & Prockter, 2014; F. Nimmo et al., 2003).

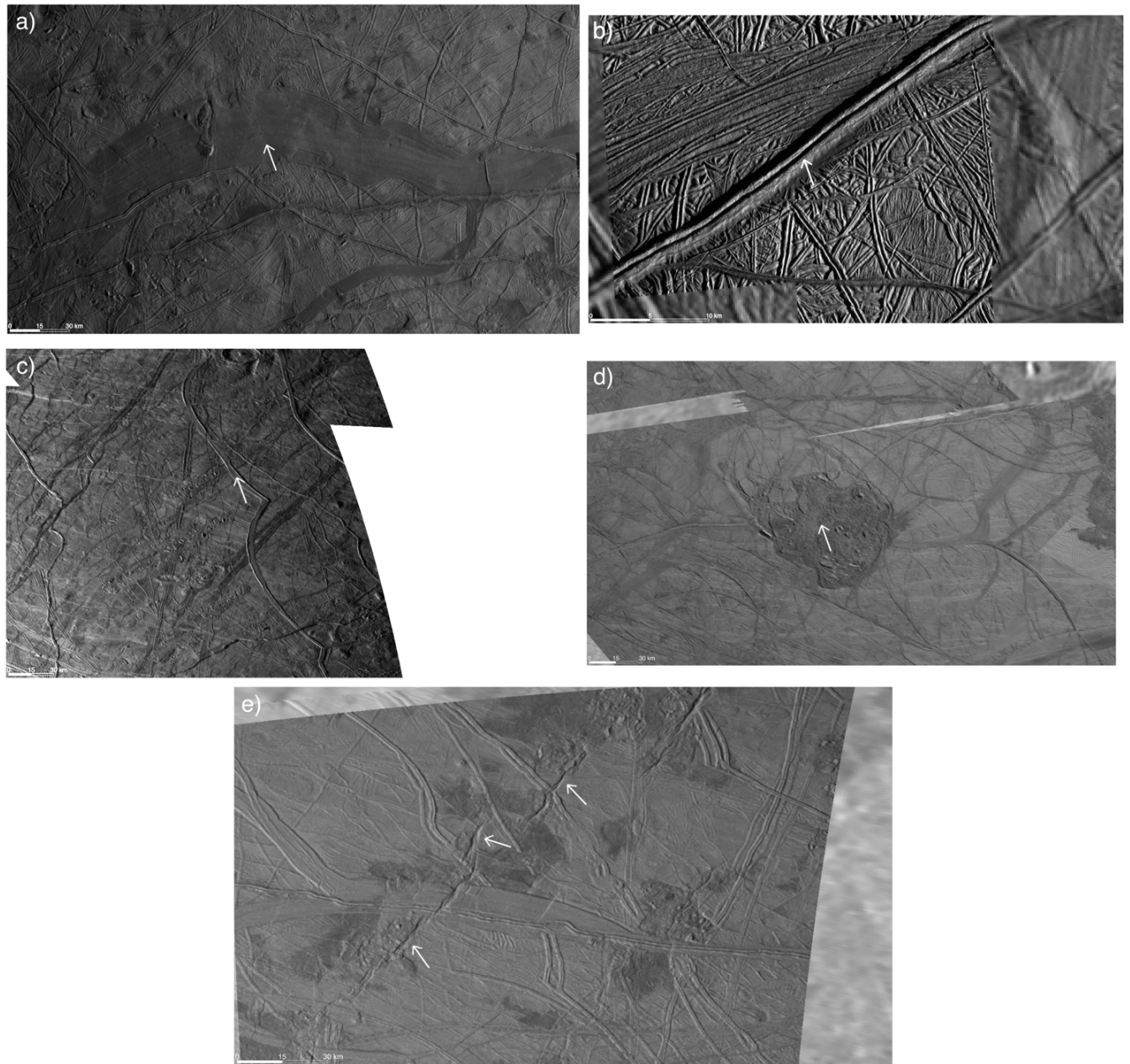
114 Double ridges (Figure 1b) are the most common tectonically related type of feature on  
115 Europa, comprising a central crack or trough flanked by two quasi-symmetric raised edifices, up  
116 to a few hundred meters high and less than 5 km wide (Kattenhorn & Hurford, 2009). These  
117 ridges may extend for hundreds of kilometers and include some of the oldest features visible on  
118 the surface, with frequent cross-cutting implying numerous formation cycles over Europa's  
119 history. Numerous double ridges follow cycloidal paths (i.e., chains of arcs) across the surface:  
120 as the tidal stress field changes through time, propagation of tensile cracks occurs (Greenberg &  
121 Sak, 2014). Double ridges may indicate intrusions of near-surface liquid water (Dombard et al.,  
122 2013; Johnston & Montési, 2014), shear heating (Han & Showman, 2008; Kalousova et al.,  
123 2016; Nimmo & Gaidos, 2002), eruptions (Fagents, 2003), or direct extrusion of recently frozen  
124 ocean water by fractures opening and closing under tidal stresses (Greenberg et al., 2003). More  
125 recent studies suggest how double ridges might be formed through a combination of shear  
126 heating and refreezing, pressurization and fracturing of shallow water reservoirs (e.g., Culberg et  
127 al., 2022).

128 Cycloids (Figure 1c) are linked, arcuate fractures that form hundreds to thousands of  
129 kilometres long chains of multiple, concatenated segments (Kattenhorn & Hurford, 2009). As the  
130 daily principal tidal stresses on Europa change, cycloids are believed to form in response to that  
131 (e.g., Greenberg et al., 1998). A crack forms as the tidal stress in a given region increases and  
132 eventually exceeds the failure strength of the ice (i.e., becomes more tensile). A cycloidal path  
133 can track the changes in stress orientation with time as it propagates across Europa's surface, if  
134 the crack propagates slowly (a few km/h). When the tidal stress decreases, propagation ceases,  
135 completing an arc (Rhoden et al., 2021).

136 Chaotic terrains are (Figure 1d), on Europa, geologically very young and extensively  
137 disrupted surface features, interpreted as reflecting recent interaction with shallow subsurface  
138 material (Chivers et al., 2021; Collins & Nimmo, 2009; B. E. Schmidt et al., 2011). Leading-  
139 hemisphere chaos regions have recently been shown to be compositionally distinct from their  
140 surroundings, probably indicating contributions from endogenous sodium chloride sourced from  
141 the subsurface ocean (Trumbo et al., 2019a, 2019b, 2022).

142 Fossae (Figure 1e) are long, narrow depressions. The term is used for topographic  
143 features that occur on extraterrestrial planetary surfaces, whose exact origin is uncertain,  
144 although they are thought to be the result of predominantly extensional tectonic processes  
145 (Schenk et al., 2020).

146



147

148 Figure 1. Examples of several geological features on Europa. White arrows point at each terrain  
149 type described in the text: a) Band (panel centered at 6°S, 122°E); b) Double ridge (panel  
150 centered at 14°N, 86°E); c) Cycloid (panel centered at 53°N, 73°W); d) Chaos (panel centered at  
151 46°S, 178°E); e) Fossa (panel centered at 43°N; 5°E). North is up in all panels.

152

153 Here we investigate the region around Ménec Fossae on Europa (centered at 51°S,  
154 177°W; on Europa's trailing hemisphere) for which we produced high-resolution  
155 photoclinometrically-derived (Lesage et al., 2021; Schenk & Pappalardo, 2004) digital terrain

156 models (DTMs) and a geomorphological-structural map (scale 1:80,000). This area is of  
 157 particular interest, as it displays the interaction between bands, double ridges, chaotic terrains  
 158 and fossae, which might share common formation processes, potentially related to shear heating  
 159 and refreezing, pressurization and fracturing of shallow water reservoirs (Culberg et al., 2022).

160 Our results suggest that this area of Europa has undergone transtensional (strike-slip with  
 161 a major extensional component) tectonic activity, as indicated by the orientation and relationship  
 162 of the tectonic features present. Such tectonic setting has possibly created a pathway facilitating  
 163 the ascent of subsurface material, especially volatiles (Aydin, 2006). These results, together with  
 164 ongoing work on other areas of Europa's surface, will help ascertain the most likely regions on  
 165 Europa in which to find fresh material, representative of the subsurface ocean, and be used as  
 166 input data for dust ejecta trajectory models that will ultimately assist the time-of-flight mass  
 167 spectrometer Surface Dust Analyzer (SUDA), onboard the upcoming *Europa Clipper* mission, in  
 168 compositionally mapping Europa's surface (Goode et al., 2021; Kempf et al., 2014; Postberg et  
 169 al., 2011).

170

## 171 2 Materials and Methods

172 DTMs of the selected areas have been produced using the photoclinometry (PC)  
 173 technique (e.g., Schenk & Pappalardo, 2004), through the Ames Stereo Pipeline (ASP) Shape-  
 174 from-Shading (SfS) tool (Beyer et al., 2018). DTMs were derived from *Galileo*'s Solid-State  
 175 Imager (SSI) images (Belton et al., 1992), which were processed through the Integrated Software  
 176 for Imagers and Spectrometers (ISIS<sup>1</sup> 4.4.0). In the final map, photogrammetrically controlled  
 177 image mosaics were used as background (Bland et al., 2021a). For the processing of *Galileo* SSI  
 178 raw image data, we used the updated SPICE smithed kernels, and projected the processed data  
 179 on a spheroid with radius of 1560.800 km (i.e., the IAU-defined mean radius for Europa) which  
 180 is therefore also the DTMs' reference height (Bland et al., 2021a). The PC/SfS technique  
 181 overcomes the lack, on Europa, of having the same surface area covered by two or more images  
 182 for traditional stereophotogrammetry DTMs' production. The smoothness parameter  $\mu$  of the SfS  
 183 tool, which weighs the smoothness of the resulting DTM and depends on surface properties,  
 184 plays an important role and can vary the results significantly: optimal  $\mu$  values with a good S/N  
 185 ratio of the resulting DTM need to be found by trial and error, where different values need to be  
 186 applied for each image (a detailed description of how  $\mu$  affects the DTMs results can be found in  
 187 Lesage et al., 2021). Manual quality checks have been conducted through features' height  $H$   
 188 estimation based on shadow length  $L$  and solar elevation angle  $\alpha$ :  $H = L \tan(\alpha)$ . The SfS tool  
 189 assumes uniformity in albedo and photometric parameters across the whole image, based on the  
 190 reflectance model used. Even though such properties can change at regional or local scales, the  
 191 overall uncertainties on the SfS DTMs vertical resolution are likely not more than 10-15%, as  
 192 previously discussed in the literature (Bierhaus & Schenk, 2010; Bland et al., 2021b; Lesage et  
 193 al., 2021; Schenk et al., 2020; Schenk & Pappalardo, 2004). We further conducted  
 194 geomorphological-structural mapping of the selected areas on SSI images 9926r and 9939r in  
 195 stereographic projection using QGIS<sup>2</sup> and the Mappy plugin<sup>3</sup> (image frames resolution of ~40  
 196 m/pixel, which corresponds to a map scale of 1:80,000), units were distinguished based on

<sup>1</sup> <https://isis.astrogeology.usgs.gov/7.0.0/index.html>

<sup>2</sup> QGIS.org, 2022. QGIS Geographic Information System. QGIS Association. <http://www.qgis.org>

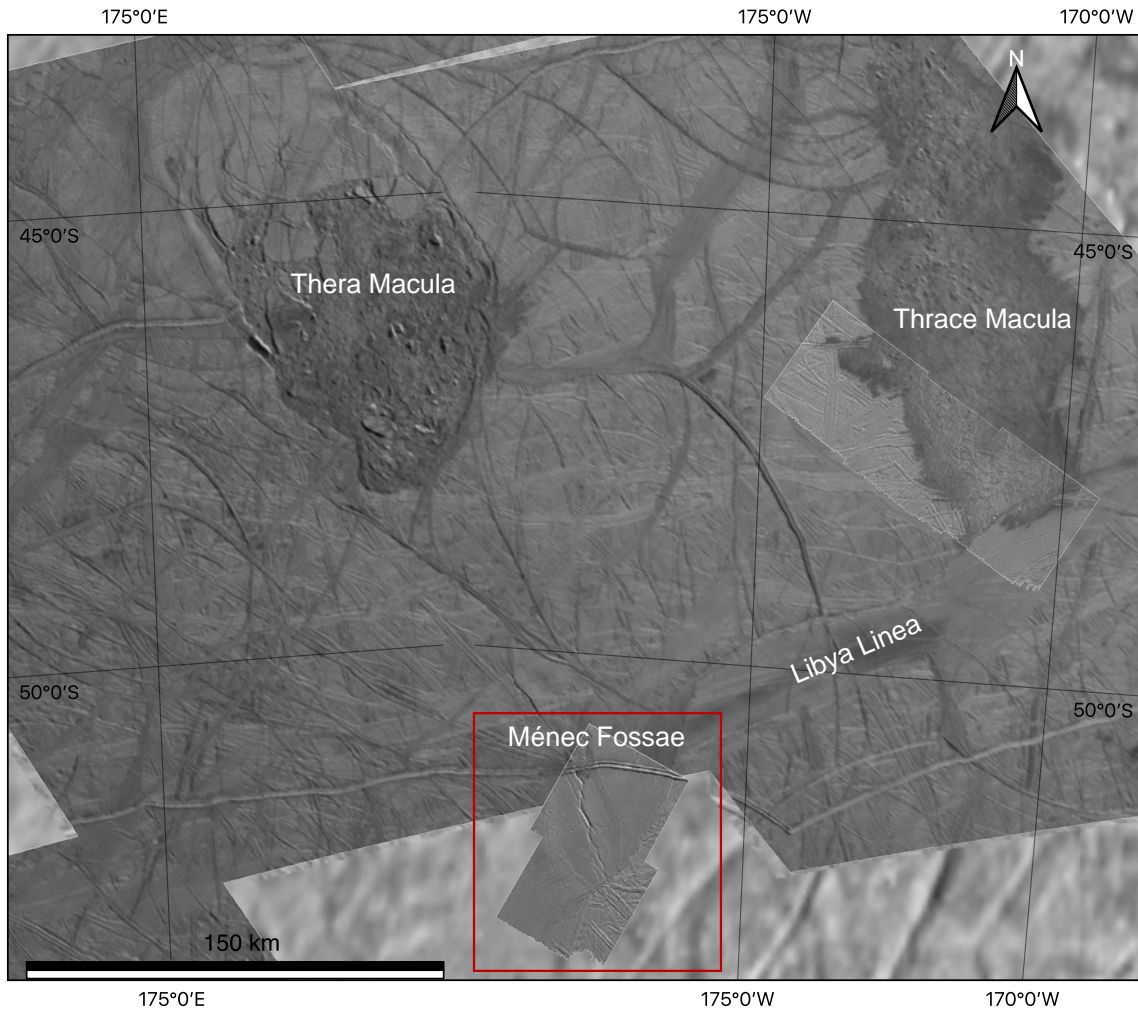
<sup>3</sup> <https://zenodo.org/record/5524389>

197 morphology and albedo differences. Tectonic linear features such as faults were identified based  
 198 on distinctive morphologies such as scarps, paired with topographical analysis of the DTMs.

199 **3 Results**

200 Méneç Fossa is located in the southern trailing hemisphere of Europa, nearby Thera and  
 201 Thrace Maculae (Figure 2). We produced high-resolution DTMs of the study area (Figure 3),  
 202 through the SfS technique described in Section 2.

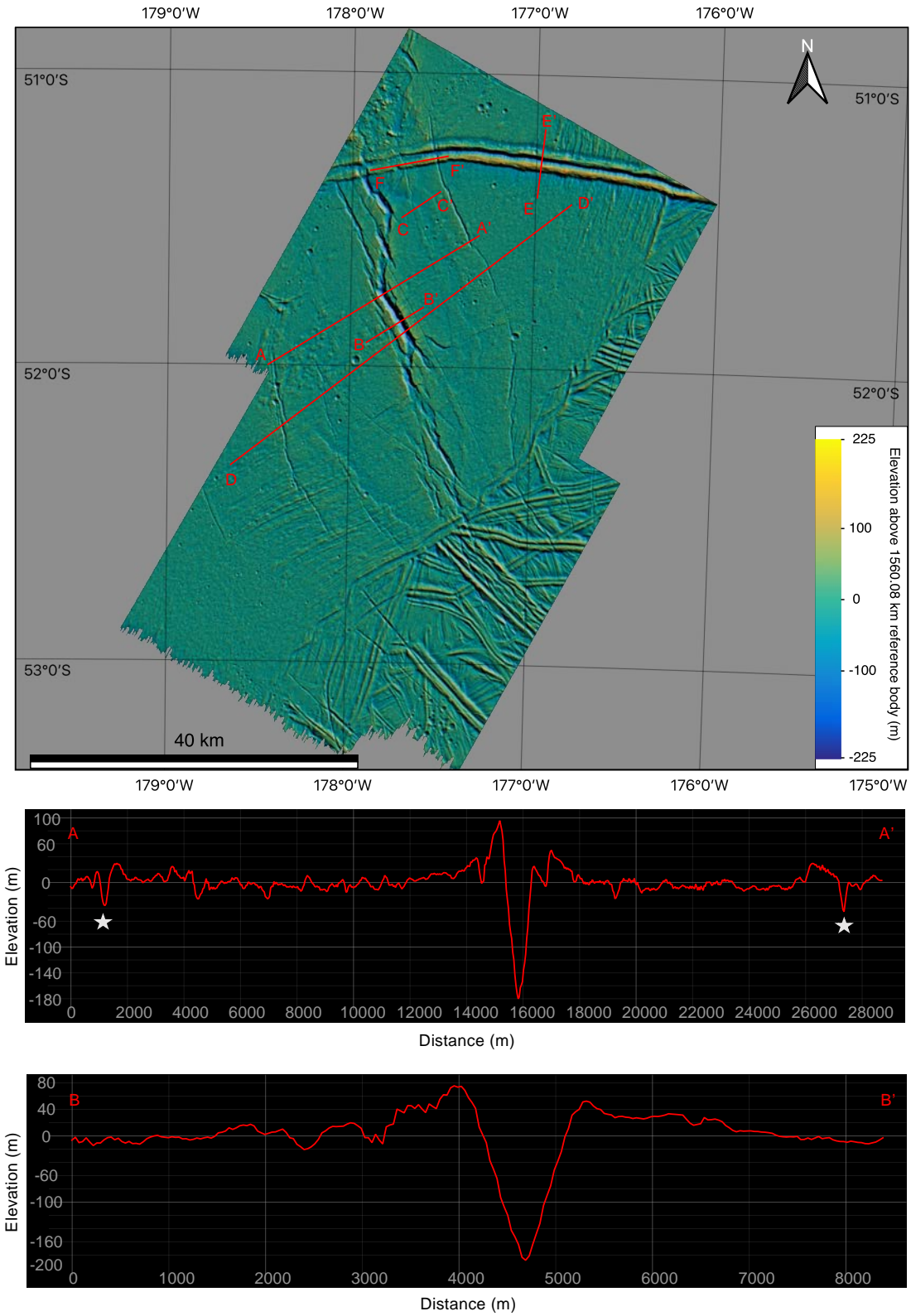
203



204

205 Figure 2. Regional map on photogrammetrically controlled *Galileo* SSI image mosaics, the red  
 206 box depicts the study area. To the NW, Thera Macula is recognizable, while Thrace Macula is  
 207 located to the NE. Libya Linea, a large-scale smooth band, continues along a NE-SW into Méneç  
 208 Fossae.

209

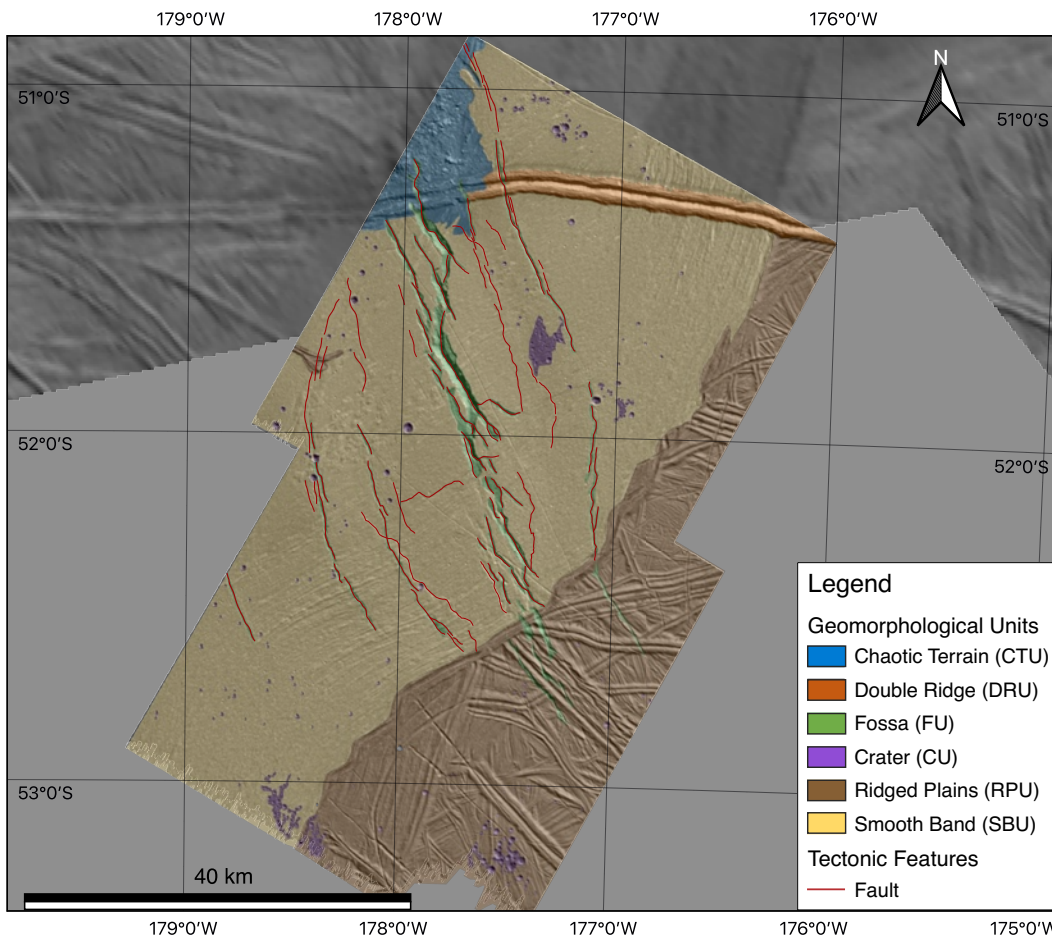
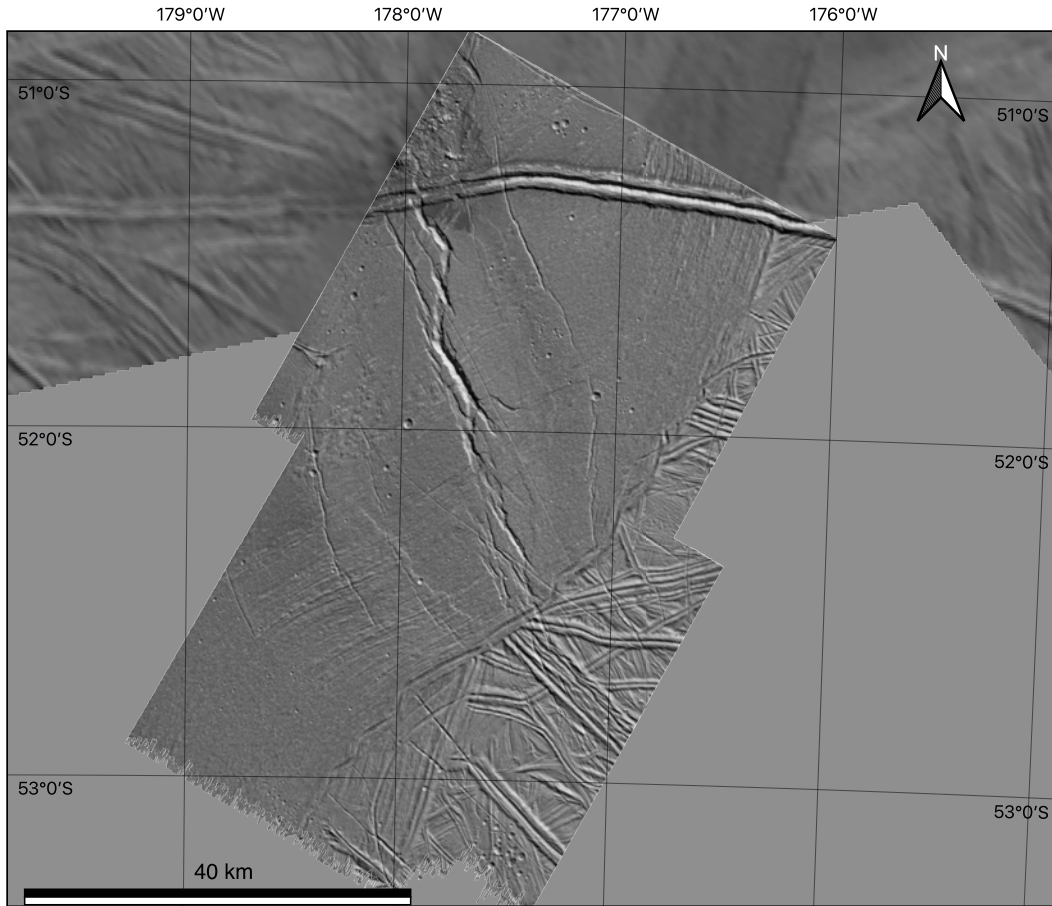


210

211 Figure 3. (Top) Regional DTM of Méneç Fossae, individual DTMs are of 9926r and 9939r  
 212 *Galileo* SSI image frames, later mosaicked together. The DTM has smoothness parameter ( $\mu$ )

213 values of 0.004 for the southern 9926r image frame and of 0.1 for the northern 9939r image  
214 frame. Image centered at 52°S, 177°W. Several elevation profile paths are shown, A-A' and B-  
215 B' profiles are displayed in the bottom panel (vertical exaggeration factor 1), the others are in  
216 Figure 5. (Bottom) Elevation profiles. The main central depression reaches depths of ~200 m and  
217 is ~1 km wide along the elevation profile (detail in B-B'), with slope angles values of ~20-25° on  
218 the gentler southern side and of ~30-35° on the steeper northern side. Several minor depressions,  
219 flanking the main one, reach depths of 40-50 m (examples as star symbols in profile A-A').  
220

221 We further conducted geomorphological analysis paired with fault mapping, resulting in  
222 a geomorphological-structural map of the Ménec Fossae area at a scale of 1:80,000 (Figure 4).  
223 We could distinguish among six different geomorphological units (Chaotic Terrain, Double  
224 Ridge, Fossa, Crater, Ridged Plains and Smooth Band), which are hereafter described and  
225 interpreted.  
226



228 Figure 4. (Top) Image mosaic of *Galileo* SSI 9926r and 9939r frames centered at 52°S, 177°W,  
229 displaying the area of Ménece Fossae. Photogrammetrically controlled SSI image mosaics as  
230 background. (Bottom) Geomorphological-structural map of Ménece Fossae. A detailed  
231 interpretation of the tectonic features is given in the text and in Figure 6.

232

### 233 3.1 Description and interpretation of geomorphological units

#### 234 3.1.1 Chaotic Terrain Unit

235 The Chaotic Terrain Unit (CTU) is formed by high albedo blocks or polygons of pre-  
236 existing crustal material, tens of meters to 1-2 km in size, within a low albedo hummocky matrix  
237 (Greeley et al., 2000; Leonard et al., 2018) that, in the studied area lie generally at the same or  
238 lower level than the surrounding units, with locally higher crustal blocks (Figure 3).

#### 239 3.1.2 Double Ridge Unit

240 The Double Ridge Unit (DRU) consists of two subparallel quasi-linear and symmetric  
241 topographically high landforms of relatively high albedo. The landforms are rounded to  
242 triangular in cross-section and separated by a trough that contains lower albedo material. In the  
243 northwestern part of the map (Figure 4), the DRU has been incorporated into the CTU, with a  
244 resulting topographic drop in the corresponding area, and therefore predates such unit (Figures 3  
245 and 5f). It is important to note that the mapped double ridge exhibits flexural bulges and flanking  
246 troughs along both its sides (Figure 5e), characteristics previously described by Dombard et al.  
247 (2013) who suggested that those double ridges displaying them originate from shallow water  
248 bodies. On the regional map (Figure 2), it appears clear how the DRU patch is part of a much  
249 bigger cycloid structure (i.e., it is a cycloidal double ridge, Hoppa et al., 1999). Nevertheless, it  
250 must be taken into account that at the map scale and within the Ménece Fossae setting, this DRU  
251 patch has all geomorphological characteristic of a European double ridge. Therefore we consider  
252 it as such, although this could be deemed as a cycloidal ridge on a wider context. Furthermore, in  
253 the literature there is a shared consensus to consider cycloidal ridges (such as the one part of  
254 DRU in the mapped area) as most likely having the same formation process as double ridges  
255 (Culberg et al., 2022; Figueredo & Greeley, 2004; Greenberg & Sak, 2014; Hoppa et al., 1999;  
256 Johnston & Montési, 2014).

#### 257 3.1.3 Fossa Unit

258 The Fossa Unit (FU) is formed by topographically low quasi-linear landforms that have a  
259 low albedo appearance. In the mapped area these depressions have steep sides, v-shaped cross  
260 sections and many exhibit terraces; the major of such features reach depths up to ~200 m. Since  
261 it crosscuts all other mapped units, and therefore postdates them, the FU is interpreted as the  
262 youngest unit in this area.

#### 263 3.1.4 Crater Unit

264 The Crater Unit (CU) consists of moderately high albedo material comprising a crater's  
265 floor, wall, and raised rim. It is interpreted as material excavated and/or deposited during impact  
266 events. Given their clustered appearance and the lack of significant ejecta blanket deposits,  
267 craters in this area of Europa have previously been interpreted as being secondary, i.e., craters

268 formed by material ejected from large primary impact craters (Bierhaus & Schenk, 2010;  
269 Bierhaus et al., 2005; Singer et al., 2013).

### 270 3.1.5 Ridged Plains Unit

271 The Ridged Plains Unit (RPU) is characterized by a series of small-scale (~200-500 m in  
272 width) high-albedo ridges which can be anywhere from sub-parallel to overlapping, and in  
273 several cases in multiple orientations. In general, on Europa's surface, ridged plains are one of  
274 the oldest terrain types (Figueredo & Greeley, 2004; Greeley et al., 2000; Leonard et al., 2020;  
275 Pappalardo et al., 1999; Prockter et al., 1999). This is the case in the mapped area as well, as they  
276 are crosscut by all the units they are in contact with.

### 277 3.1.6 Smooth Band Unit

278 The Smooth Band Unit (SBU) consists of either very subdued ridges and troughs or  
279 material with little or no structure. In the mapped area, the SBU is a portion of the very large  
280 structure Libya Linea, which extends over thousands of km (Figure 2). Smooth bands are  
281 interpreted as regions of crustal extension in which the low relief and lack of internal structure  
282 can be due to small-scale fracturing or the emplacement of infilling material (e.g., Prockter et al.,  
283 2002)

## 284 3.2 Stratigraphic sequence

285 Based on the crosscutting relationships among the different geomorphological units, we  
286 could determine the following sequence of events (numbered, in brackets):

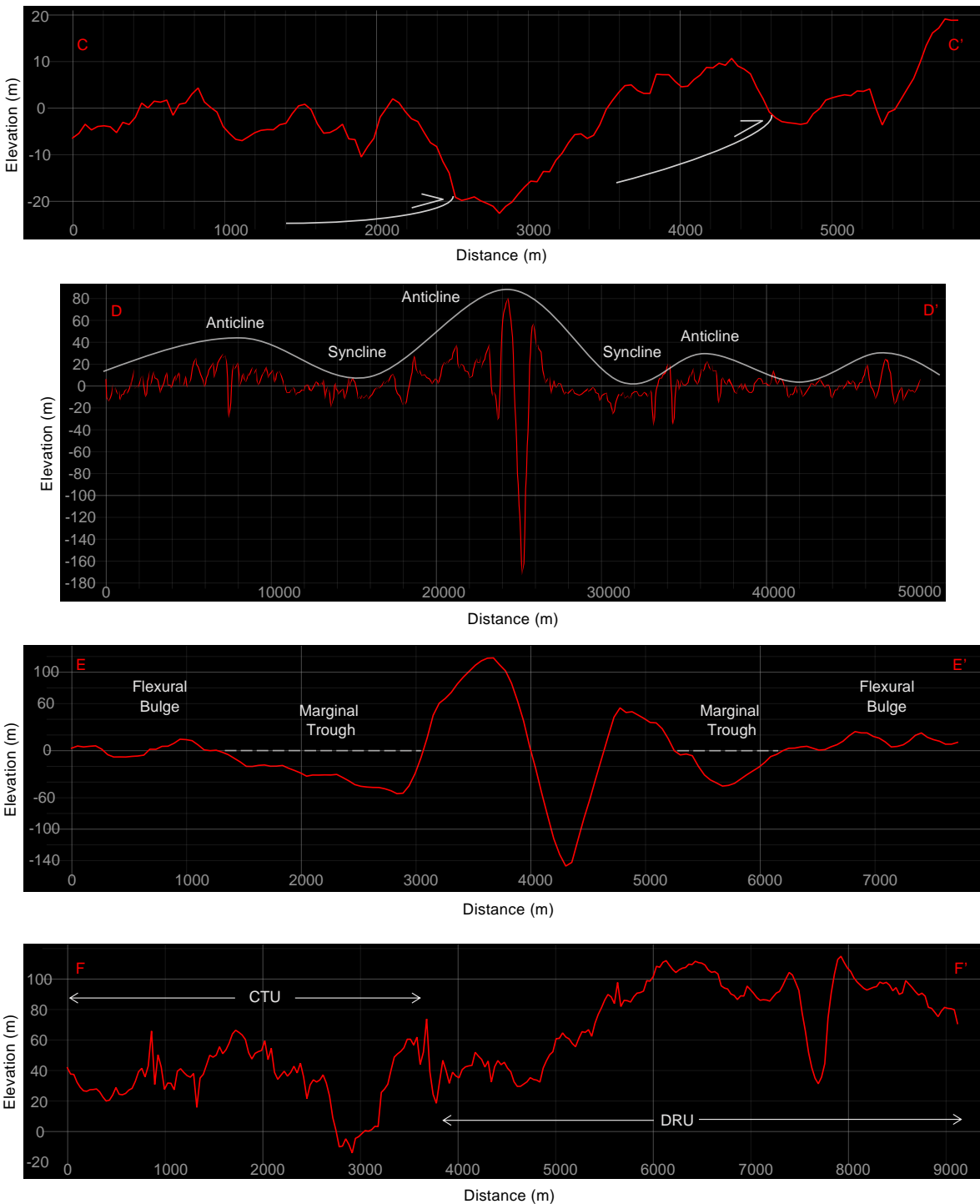
- 287 • RPU is the oldest terrain (1), as it occurs in most regions of Europa (Leonard et  
288 al., 2020).
- 289 • SBU (2), i.e., a portion of Libya Linea, superimpose the RPU.
- 290 • Subsequently, the DRU (3) has formed; in the north-western edge of the mapped  
291 area, this unit has been incorporated in the CTU (4) which therefore postdates it.
- 292 • Ultimately, the FU (5) crosscuts all the other units it is in contact with. The CU  
293 (6) is located on top of all other units, while there is no patch of such unit in  
294 contact with the FU, thus the cratering events were older or at least concurrent to  
295 the FU formation.

296  
297 Such stratigraphic sequence follows the typical three-stage development on Europa: the initial  
298 formation of ridged plains, followed by band-like features and ultimately the imposition of chaotic  
299 terrains (Leonard et al., 2020).

## 300 3.3 Tectonic features

301 Different types of faults have been identified and mapped. Note that many other faults are  
302 located in the south-eastern part of the mapped area, within the RPU (Figure 4). Considering that  
303 this is the oldest of the mapped units, these faults belong to a much older and likely different  
304 tectonic regime. We therefore did not distinguish them in the map and consider them as being  
305 part of the RPU's general rugged appearance.

306 Most of the mapped faults display both extensional and strike-slip characteristics, such as  
307 clear distinctive elevation drops yet with very steep sides and no clear hanging wall - foot wall  
308 distinction (uncommon in purely extensional faults), along with *en échelon* disposition (Figures  
309 3 and 4); we therefore consider them as transtensional faults (i.e., strike-slip features with an  
310 extensional component). The most prominent ones in terms of topographic drop have been  
311 mapped as part of the FU (Figure 4). These faults follow a roughly NW-SE trend and are  
312 distributed within three zones: around the center of the mapped area, where Méneç Fossa *s.s.*  
313 takes part most of the extensional component, spread along several quasi-parallel *en échelon*  
314 troughs, which become anastomosing towards their SE tips, while reaching depths up to ~200 m  
315 (Figure 3). These features are located along the anticline crest of a long-wavelength fold system,  
316 as previously observed on SSI image data by (Prockter & Pappalardo, 2000) and further  
317 confirmed in this study through the newly available topographic information contained in the  
318 DTM (Figure 5d). On both sides of these central features, at distances up to 10-15 km, there are  
319 two other sets of subsidiary *en échelon* transtensional faults also aligned along NW-SE trends,  
320 subparallel to the main central features. These subsidiary faults have elevation drops of ~40-50  
321 m in their deepest portions (Figure 3). Along with such structures, few other features have been  
322 identified. These are flanking the main central feature as well, along similar orientations. They  
323 display a clear increase in elevation, along a roughly SW-NE axis, followed by abrupt  
324 asymmetrical scarps, with lobate planform geometries (Figures 3 and 5c and 6), all  
325 characteristics typical of compressive faults (Prockter & Pappalardo, 2000) on Earth and other  
326 planetary bodies (e.g., Mars, Titan). We therefore consider them as compressive tectonic features  
327 (i.e., thrust faults).



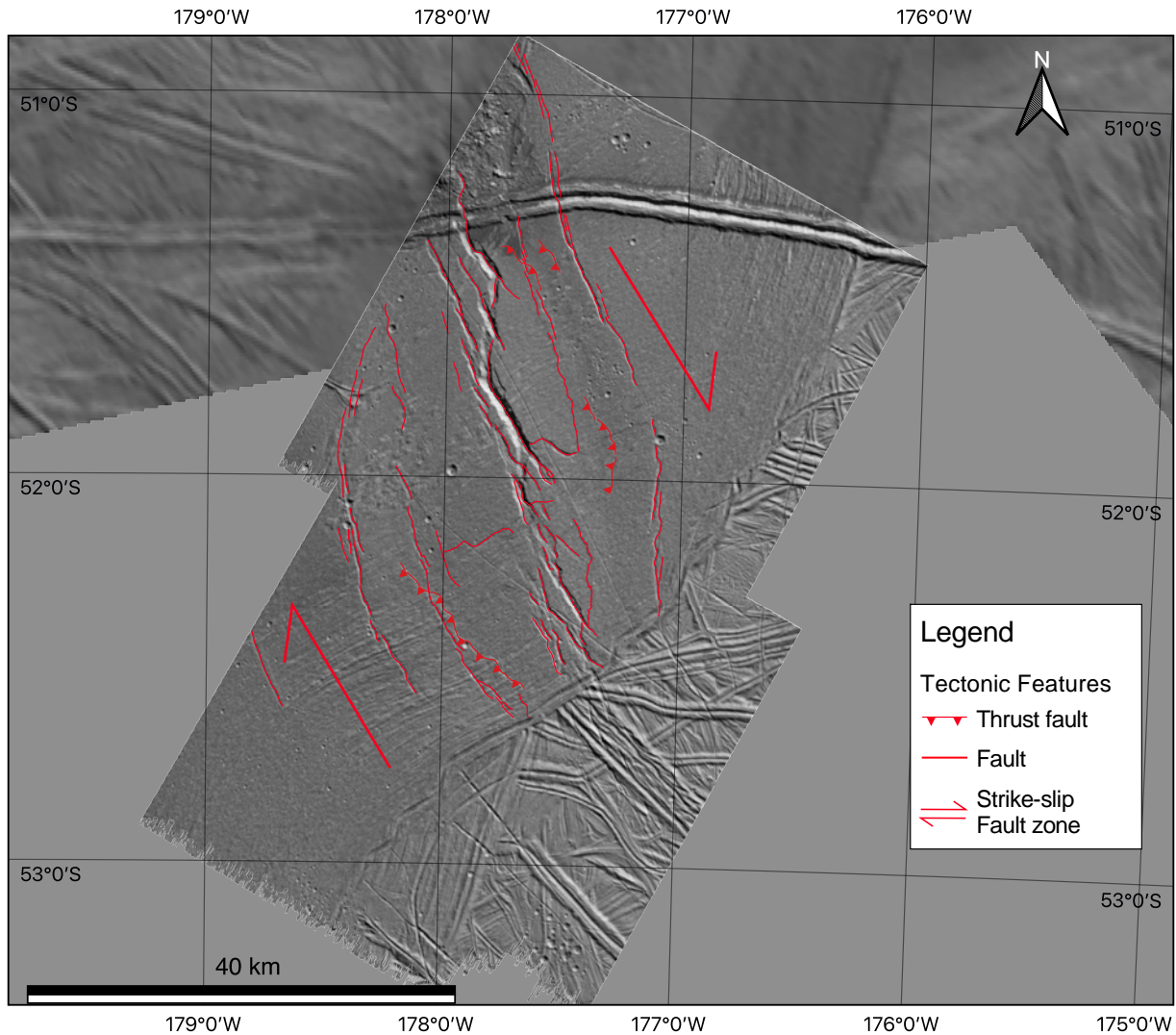
328

329 Figure 5. Elevation profiles along the DTM at various locations, profiles' paths are displayed in  
 330 Figure 3. Vertical exaggeration factor is 1 in all panels. (C-C') Examples of mapped thrust faults,  
 331 with hypothetical fault traces sketched in white. The two thrusts seem to follow a typical  
 332 imbricate fan geometry. (D-D') Long distance profile displaying the long-wavelength fold  
 333 system discussed in Section 3.3. (E-E') Detail of the double ridge (DRU), depicting the observed

334 marginal troughs and flexural bulges that support the shallow water reservoir's hypothesis as its  
 335 origin (Section 3.1.2). (F-F') Detail of the CTU-DRU transition, showing the elevation drop  
 336 corresponding to the incorporation of the DRU in the CTU, proving the DRU relative older  
 337 formation timing (Section 3.1.2).

338

339



340

341 Figure 6. Proposed structural setting in the area of Ménece Fossae, image centered at 52°S,  
 342 177°W. The right-lateral strike-slip faulting controls the deformation along a wide shear zone,  
 343 generating several extensional and transtensional features (marked together in the legend for ease  
 344 of use of the structural map) and few compressive structures, in a predominantly transtensional

345 tectonic setting. Local portions have a larger compressional component, resulting in folding (see  
346 Figure 5) and thrust faulting.

347

### 348 **3 Discussion and conclusions**

349 Several formation hypotheses have been previously proposed for the area of Ménéce  
350 Fossae. Prockter & Pappalardo (2000) consider it as a regional scale anticline (upward convex)  
351 fold's crest flanked by small reverse faults, which are inferred to mark syncline (upward  
352 concave) folds' hinges. In this case, the folding and associated small scale thrust faulting would  
353 imply that compression was, or is, ongoing in this area of Europa, which would locally  
354 compensate for the ubiquitous extension observed on this Jupiter's icy moon. More recently, it  
355 has been suggested (Schenk et al., 2020) that Ménéce Fossa is part of a set of *en échelon* fissures  
356 associated with True Polar Wander (TPW) of the ice shell (Schenk et al., 2008), involving a 70°  
357 global rotation of surface features. The authors consider these features as sets of multiple parallel  
358 faults in which most of the extension is confined within a single narrow central feature. The  
359 fissures are also thought to be closely associated with buckling or tilting of the surface by a few  
360 tens of meters within the deformation zone. Other features on Europa associated with TPW  
361 (Schenk et al., 2020) include the same terrain type, displaying similar geomorphological and  
362 structural characteristic as Ménéce Fossae (Kermario Fossae - 43°N, 5°E; Kerlescan Fossae - 3°N,  
363 238°W).

364 Based on observations on geomorphology and topography of the Ménéce Fossae area, our  
365 novel hypothesis for its formation mechanisms involves transtensional tectonics (Figure 6) above  
366 a shallow water reservoir. Such hypothesis considers the two main previous models on this area,  
367 described above (Prockter & Pappalardo, 2000; Schenk et al., 2020), and combines them with  
368 proposed mechanisms for the formation of different surface features on Europa, including  
369 chaotic terrains and double ridges (e.g., Chivers et al., 2021; Craft et al., 2016; Culberg et al.,  
370 2022; Dombard et al., 2013; Kalousova et al., 2016; B. E. Schmidt et al., 2011). These last  
371 contributions all invoke the emplacement of shallow water bodies within the ice shell to generate  
372 the various surface expressions they focus on. In particular, through a comparison with an  
373 analysis of an Earth's double ridge in Greenland, Culberg et al. (2022) show how double ridges  
374 might form via refreezing, pressurization and fracturing of shallow water reservoirs, potentially  
375 induced by shear heating (Han & Showman, 2008; Kalousova et al., 2016; Nimmo & Gaidos,  
376 2002). Moreover, our observations (Section 3.1.2) on the flexural bulges and flanking troughs  
377 along the sides of the mapped double ridge (DRU), further strengthen the case for it originating  
378 from a shallow water body. In fact, Dombard et al. (2013) suggest how shallow water reservoirs  
379 must be involved in double ridges' formation in order to explain the aforementioned flanking  
380 features, where those are present. These processes could also operate in conjunction with other  
381 proposed double ridges' formation mechanisms, such as shear heating (Johnston & Montési,  
382 2014).

383 In this study, our analyses on the geomorphological units and tectonic features of the  
384 Ménéce Fossae area are consistent with such models. We observe a deep central feature (Ménéce  
385 Fossa s.s.) that takes up most of the extension, flanked by numerous quasi-parallel subsidiary  
386 extensional and strike-slip faults and few thrust faults, all in a deformation zone of 20-30 km (see  
387 Section 3.3). We propose that such a tectonic setting is generated within a right-lateral strike-slip

388 fault zone, with a major contribution from an extensional component, i.e., a transtensional  
389 tectonic setting (Figure 6). The shear heating related to such a tectonic setting possibly led to the  
390 formation of a shallow water reservoir within the ice shell, that in turn could have generated the  
391 DRU first and the CTU later (timing based on their crosscutting relationships). Such a scenario is  
392 consistent with the  $70^\circ$  global rotation of surface features through TPW proposed by Schenk et  
393 al. (2020), to explain the abrupt different orientation of the DRU (E-W) and the CTU and FU  
394 (NW-SE), which fits to a  $70^\circ$  rotation. The shallow water reservoir likely responsible for the  
395 DRU and CTU formation would have then been involved in such a rotation; its ultimate  
396 expression would be the FU and the associated faulting, which are a display on the surface of  
397 shearing through transtensional tectonics. Most formation models have calculated depths of 1-5  
398 km for the emplacement of shallow water reservoirs beneath various geological features  
399 (lenticulae, chaos, double ridges, Chivers et al., 2021; Craft et al., 2016; Dombard et al., 2013;  
400 Johnston & Montési, 2014; Kalousova et al., 2016; Manga & Michaut, 2017; B. E. Schmidt et  
401 al., 2011), with estimates varying depending on the adopted thickness value of Europa's ice  
402 shell. We therefore assume a water reservoir's emplacement depth within such range in the study  
403 area, in agreement with the observed lowest elevations at Méneç Fossae of  $\sim -200$  m (see Section  
404 3.3). Compositional information is not available for the study area, as there are no *Galileo* Near  
405 Infrared Mapping Spectrometer (NIMS) data at this location. Having such kind of information  
406 would have been essential for detailed characterization of fresh subsurface material potentially  
407 emplaced by the Méneç Fossae fault system.

408 Transtensional tectonic features are widely common on Earth, mainly within large-scale  
409 strike-slip settings (Donzé et al., 2021). They have also been observed on terrestrial planets (e.g.,  
410 Mars, Andrews-Hanna et al., 2008; G. Schmidt et al., 2022) and on other ocean worlds,  
411 Ganymede (e.g., Rossi et al., 2018), Enceladus (e.g., Rossi et al., 2020), and Titan (e.g.,  
412 Burkhard et al., 2022; Matteoni et al., 2020). Several other examples exist on Europa as well,  
413 such as along Agenor Linea in the southern trailing hemisphere and Astypalaea Linea in the  
414 south polar region (Hoyer et al., 2014; Kattenhorn & Prockter, 2014; Tufts et al., 1999). In  
415 transtensional tectonic regimes, minor compressional features are common and expected (Fossen  
416 et al., 1994; Petit, 1987). In this context, the small thrust faults observed are consistent as being  
417 formed within a predominantly transtensional setting. This hypothesis does not rule out that of  
418 Prockter & Pappalardo (2000), which consider such thrust faults as marking synclinal folds'  
419 hinges and Méneç Fossa s.s. as a regional scale anticline's crest within the same fold system. In  
420 fact, in transtensional settings folding (on an oblique axis with respect to the major strike-slip  
421 fault zone, as we observe in the study area) is also common (Fossen et al., 1994).

422 We conclude that Méneç Fossa and its surroundings have been shaped by transtensional  
423 tectonic activity, most likely above a shallow water reservoir, whose emplacement has been  
424 potentially induced by shear heating. This model explains how an intriguing area of Europa,  
425 displaying several major terrain types, might have formed through one single major mechanism,  
426 while further strengthening the case for widely distributed shallow water reservoirs within  
427 Europa's ice shell.

428

429

430

431 **Acknowledgments**

432 The research leading to this manuscript received funding from the European Research Council  
 433 (ERC) under the European Union's Horizon 2020 research and innovation programme (ERC  
 434 Consolidator Grant 724908-Habitat OASIS)

435

436 **Open Research**

437 Data Availability Statement

438

439 *Galileo*'s SSI data used in this manuscript can be accessed from the PDS Cartography and  
 440 Imaging Science Node via <https://pds-imaging.jpl.nasa.gov/volumes/galileo>, while the SSI  
 441 photogrammetrically-corrected basemap mosaics can be accessed from the USGS Astrogeology  
 442 website via <https://doi.org/10.5066/P9VKKK7C>. The Digital Terrain Model (Figure 3) and data  
 443 of the geomorphological-structural map (Figure 4) produced are available on TRR 170-DB  
 444 (Matteoni, 2022).

445

446 **References**

- 447 Anderson, J. D., Schubert, G., Jacobson, R. A., Lau, E. L., Moore, W. B., & Sjogren, W. L.  
 448 (1998). Europa's Differentiated Internal Structure: Inferences from Four Galileo  
 449 Encounters. *Science*, *281*(5385), 2019–2022. <https://doi.org/10.1126/science.281.5385.2019>
- 450 Andrews-Hanna, J. C., Zuber, M. T., & Hauck, S. A. (2008). Strike-slip faults on Mars:  
 451 Observations and implications for global tectonics and geodynamics. *Journal of*  
 452 *Geophysical Research*, *113*(E8), E08002. <https://doi.org/10.1029/2007JE002980>
- 453 Aydin, A. (2006). Failure modes of the lineaments on Jupiter's moon, Europa: Implications for  
 454 the evolution of its icy crust. *Journal of Structural Geology*, *28*(12), 2222–2236.  
 455 <https://doi.org/10.1016/j.jsg.2006.08.003>
- 456 Barr, A. C., & Pappalardo, R. T. (2005). Onset of convection in the icy Galilean satellites:  
 457 Influence of rheology. *Journal of Geophysical Research*, *110*(E12), E12005.  
 458 <https://doi.org/10.1029/2004JE002371>
- 459 Běhounková, M., Tobie, G., Choblet, G., Kervazo, M., Melwani Daswani, M., Dumoulin, C., &  
 460 Vance, S. D. (2021). Tidally Induced Magmatic Pulses on the Oceanic Floor of Jupiter's  
 461 Moon Europa. *Geophysical Research Letters*, *48*(3), 1–11.  
 462 <https://doi.org/10.1029/2020GL090077>
- 463 Belton, M. J. S., Klaasen, K. P., Clary, M. C., Anderson, J. L., Anger, C. D., Carr, M. H., et al.  
 464 (1992). The Galileo Solid-State Imaging experiment. *Space Science Reviews*, *60*(1–4), 413–  
 465 455. <https://doi.org/10.1007/BF00216864>
- 466 Beyer, R. A., Alexandrov, O., & McMichael, S. (2018). The Ames Stereo Pipeline: NASA's  
 467 Open Source Software for Deriving and Processing Terrain Data. *Earth and Space Science*,  
 468 *5*(9), 537–548. <https://doi.org/10.1029/2018EA000409>
- 469 Bierhaus, E. B., & Schenk, P. M. (2010). Constraints on Europa's surface properties from  
 470 primary and secondary crater morphology. *Journal of Geophysical Research E: Planets*,

- 471 115(12), 1–17. <https://doi.org/10.1029/2009JE003451>
- 472 Bierhaus, Edward B., Chapman, C. R., & Merline, W. J. (2005). Secondary craters on Europa  
473 and implications for cratered surfaces. *Nature*, 437(7062), 1125–1127.  
474 <https://doi.org/10.1038/nature04069>
- 475 Bierhaus, Edward B., Zahnle, K., & Chapman, C. R. (2009). Europa’s Crater Distributions and  
476 Surface Ages. In *Europa* (pp. 161–180). University of Arizona Press.  
477 <https://doi.org/10.2307/j.ctt1xp3wdw.13>
- 478 Bland, M. T., Kirk, R. L., Galuszka, D. M., Mayer, D. P., Beyer, R. A., & Fergason, R. L.  
479 (2021). How Well Do We Know Europa’s Topography? An Evaluation of the Variability in  
480 Digital Terrain Models of Europa. *Remote Sensing*, 13(24), 5097.  
481 <https://doi.org/10.3390/rs13245097>
- 482 Bland, M. T., Weller, L. A., Archinal, B. A., Smith, E., & Wheeler, B. H. (2021). Improving the  
483 Usability of Galileo and Voyager Images of Jupiter’s Moon Europa. *Earth and Space  
484 Science*, 8(12). <https://doi.org/10.1029/2021EA001935>
- 485 Burkhard, L. M. L., Smith-Konter, B. R., Fagents, S. A., Cameron, M. E., Collins, G. C., &  
486 Pappalardo, R. T. (2022). Strike-slip faulting on Titan: Modeling tidal stresses and shear  
487 failure conditions due to pore fluid interactions. *Icarus*, 371(March 2021), 114700.  
488 <https://doi.org/10.1016/j.icarus.2021.114700>
- 489 Carr, M. H., Belton, M. J. S., Chapman, C. R., Davies, M. E., Geissler, P., Greenberg, R., et al.  
490 (1998). Evidence for a subsurface ocean on Europa. *Nature*, 391(6665), 363–365.  
491 <https://doi.org/10.1038/34857>
- 492 Chivers, C. J., Buffo, J. J., & Schmidt, B. E. (2021). Thermal and Chemical Evolution of Small,  
493 Shallow Water Bodies in Europa’s Ice Shell. *Journal of Geophysical Research: Planets*,  
494 126(5), 1–26. <https://doi.org/10.1029/2020JE006692>
- 495 Collins, G., & Nimmo, F. (2009). Chaotic Terrain on Europa. In *Europa* (pp. 259–282).  
496 University of Arizona Press. <https://doi.org/10.2307/j.ctt1xp3wdw.17>
- 497 Craft, K. L., Patterson, G. W., Lowell, R. P., & Germanovich, L. (2016). Fracturing and flow:  
498 Investigations on the formation of shallow water sills on Europa. *Icarus*, 274.  
499 <https://doi.org/10.1016/j.icarus.2016.01.023>
- 500 Culberg, R., Schroeder, D. M., & Steinbrügge, G. (2022). Double ridge formation over shallow  
501 water sills on Jupiter’s moon Europa. *Nature Communications*, 13(1), 1–10.  
502 <https://doi.org/10.1038/s41467-022-29458-3>
- 503 Dalton, J. B., Prieto-Ballesteros, O., Kargel, J. S., Jamieson, C. S., Jolivet, J., & Quinn, R.  
504 (2005). Spectral comparison of heavily hydrated salts with disrupted terrains on Europa.  
505 *Icarus*, 177(2), 472–490. <https://doi.org/10.1016/j.icarus.2005.02.023>
- 506 Dalton, J. B., Shirley, J. H., & Kamp, L. W. (2012). Europa’s icy bright plains and dark linea:  
507 Exogenic and endogenic contributions to composition and surface properties. *Journal of  
508 Geophysical Research: Planets*, 117(E3), n/a-n/a. <https://doi.org/10.1029/2011JE003909>
- 509 Dombard, A. J., Patterson, G. W., Lederer, A. P., & Prockter, L. M. (2013). Flanking fractures  
510 and the formation of double ridges on Europa. *Icarus*, 223(1), 74–81.  
511 <https://doi.org/10.1016/j.icarus.2012.11.021>

- 512 Donzé, F.-V., Klinger, Y., Bonilla-Sierra, V., Duriez, J., Jiao, L., & Scholtès, L. (2021).  
513 Assessing the brittle crust thickness from strike-slip fault segments on Earth, Mars and Icy  
514 moons. *Tectonophysics*, 805(May 2020), 228779.  
515 <https://doi.org/10.1016/j.tecto.2021.228779>
- 516 Fagents, S. A. (2003). Considerations for effusive cryovolcanism on Europa: The post-Galileo  
517 perspective. *Journal of Geophysical Research: Planets*, 108(E12), 13–1.  
518 <https://doi.org/10.1029/2003JE002128>
- 519 Figueredo, P. H., & Greeley, R. (2004). Resurfacing history of Europa from pole-to-pole  
520 geological mapping. *Icarus*, 167(2), 287–312. <https://doi.org/10.1016/j.icarus.2003.09.016>
- 521 Fossen, H., Tikoff, B., & Teysier, C. (1994). Strain modeling of transpressional and  
522 transtensional deformation. *Norsk Geologisk Tidsskrift*, 74(3), 134–145.
- 523 Goode, W., Kempf, S., & Schmidt, J. (2021). Detecting the surface composition of geological  
524 features on Europa and Ganymede using a surface dust analyzer. *Planetary and Space  
525 Science*, 208(September), 105343. <https://doi.org/10.1016/j.pss.2021.105343>
- 526 Greeley, R., Chyba, C. ~F., Head, I. I. I. J. ~W., McCord, T. ~B., McKinnon, W. ~B.,  
527 Pappalardo, R. ~T., & Figueredo, P. ~H. (2004). *Geology of Europa. Jupiter. The planet,  
528 satellites and magnetosphere.*
- 529 Greeley, Ronald, Figueredo, P. H., Williams, D. A., Chuang, F. C., Klemaszewski, J. E., Kadel,  
530 S. D., et al. (2000). Geologic mapping of Europa. *Journal of Geophysical Research:  
531 Planets*, 105(E9), 22559–22578. <https://doi.org/10.1029/1999JE001173>
- 532 Greenberg, R., & Geissler, P. (2002). Europa’s dynamic icy crust. *Meteoritics & Planetary  
533 Science*, 37(12), 1685–1710. <https://doi.org/10.1111/j.1945-5100.2002.tb01158.x>
- 534 Greenberg, R., & Sak, P. B. (2014). The ridges of Europa: Extensions of adjacent topography  
535 onto their flanks. *Earth and Planetary Science Letters*, 389, 43–51.  
536 <https://doi.org/10.1016/j.epsl.2013.12.009>
- 537 Greenberg, R., Geissler, P., Hoppa, G., Tufts, B. R., Durda, D. D., Pappalardo, R., et al. (1998).  
538 Tectonic Processes on Europa: Tidal Stresses, Mechanical Response, and Visible Features.  
539 *Icarus*, 135(1), 64–78. <https://doi.org/10.1006/icar.1998.5986>
- 540 Greenberg, R., Geissler, P., Tufts, B. R., & Hoppa, G. V. (2000). Habitability of Europa’s crust:  
541 The role of tidal-tectonic processes. *Journal of Geophysical Research: Planets*, 105(E7),  
542 17551–17562. <https://doi.org/10.1029/1999JE001147>
- 543 Greenberg, R., Hoppa, G. V., Bart, G., & Hurford, T. (2003). Tidal stress patterns on Europa’s  
544 crust. *Celestial Mechanics and Dynamical Astronomy*, 87(1–2), 171–188.  
545 <https://doi.org/10.1023/A:1026169424511>
- 546 Han, L., & Showman, A. P. (2008). Implications of shear heating and fracture zones for ridge  
547 formation on Europa. *Geophysical Research Letters*, 35(3), L03202.  
548 <https://doi.org/10.1029/2007GL031957>
- 549 Hand, K. P., & Carlson, R. W. (2015). Europa’s surface color suggests an ocean rich with  
550 sodium chloride. *Geophysical Research Letters*, 42(9), 3174–3178.  
551 <https://doi.org/10.1002/2015GL063559>

- 552 Hand, K. P., Phillips, C. B., Murray, A., Garvin, J. B., Maize, E. H., Gibbs, R. G., et al. (2022).  
553 Science Goals and Mission Architecture of the Europa Lander Mission Concept. *The*  
554 *Planetary Science Journal*, 3(1), 22. <https://doi.org/10.3847/PSJ/ac4493>
- 555 Hansen, G. B., & McCord, T. B. (2008). Widespread CO<sub>2</sub> and other non-ice compounds on the  
556 anti-Jovian and trailing sides of Europa from Galileo/NIMS observations. *Geophysical*  
557 *Research Letters*, 35(1), 2–6. <https://doi.org/10.1029/2007GL031748>
- 558 Hoppa, G. V., Tufts, B. R., Greenberg, R., & Geissler, P. E. (1999). Formation of Cycloidal  
559 Features on Europa. *Science*, 285(5435), 1899–1902.  
560 <https://doi.org/10.1126/science.285.5435.1899>
- 561 Howell, S. M. (2021). The Likely Thickness of Europa's Icy Shell. *The Planetary Science*  
562 *Journal*, 2(4), 129. <https://doi.org/10.3847/PSJ/abfe10>
- 563 Hoyer, L., Kattenhorn, S. A., & Watkeys, M. K. (2014). Multistage evolution and variable  
564 motion history of Agenor Linea, Europa. *Icarus*, 232, 60–80.  
565 <https://doi.org/10.1016/j.icarus.2013.12.010>
- 566 Hussmann, H. (2002). Thermal Equilibrium States of Europa's Ice Shell: Implications for  
567 Internal Ocean Thickness and Surface Heat Flow. *Icarus*, 156(1), 143–151.  
568 <https://doi.org/10.1006/icar.2001.6776>
- 569 Hussmann, H., Choblet, G., Lainey, V., Matson, D. L., Sotin, C., Tobie, G., & Van Hoolst, T.  
570 (2010). Implications of Rotation, Orbital States, Energy Sources, and Heat Transport for  
571 Internal Processes in Icy Satellites. *Space Science Reviews*, 153(1–4), 317–348.  
572 <https://doi.org/10.1007/s11214-010-9636-0>
- 573 Johnston, S. A., & Montési, L. G. J. (2014). Formation of ridges on Europa above crystallizing  
574 water bodies inside the ice shell. *Icarus*, 237, 190–201.  
575 <https://doi.org/10.1016/j.icarus.2014.04.026>
- 576 Kalousová, K., Souček, O., Tobie, G., Choblet, G., & Čadež, O. (2016). Water generation and  
577 transport below Europa's strike-slip faults. *Journal of Geophysical Research: Planets*,  
578 121(12). <https://doi.org/10.1002/2016JE005188>
- 579 Kattenhorn, S. A., & Hurford, T. (2009). Tectonics of Europa. In *Europa* (pp. 199–236).  
580 University of Arizona Press.
- 581 Kattenhorn, S. A., & Prockter, L. M. (2014). Evidence for subduction in the ice shell of Europa.  
582 *Nature Geoscience*, 7(10), 762–767. <https://doi.org/10.1038/ngeo2245>
- 583 Kempf, S., Altobelli, N., Briois, C., Grün, E., Horanyi, M., Postberg, F., et al. (2014). SUDA: A  
584 Dust Mass Spectrometer for Compositional Surface Mapping for a Mission to Europa.  
585 *European Planetary Science Congress 2014*, 9(EPSC2014-229). Retrieved from  
586 <http://adsabs.harvard.edu/abs/2014EPSC....9..229K>
- 587 Khurana, K. K., Kivelson, M. G., Stevenson, D. J., Schubert, G., Russell, C. T., Walker, R. J., &  
588 Polansky, C. (1998). Induced magnetic fields as evidence for subsurface oceans in Europa  
589 and Callisto. *Nature*, 395(6704), 777–780. <https://doi.org/10.1038/27394>
- 590 Kivelson, M. G., Khurana, K. K., Russell, C. T., Volwerk, M., Walker, R. J., & Zimmer, C.  
591 (2000). Galileo Magnetometer Measurements: A Stronger Case for a Subsurface Ocean at  
592 Europa. *Science*, 289(5483), 1340–1343. <https://doi.org/10.1126/science.289.5483.1340>

- 593 Leonard, E. J., Pappalardo, R. T., & Yin, A. (2018). Analysis of very-high-resolution Galileo  
594 images and implications for resurfacing mechanisms on Europa. *Icarus*, *312*, 100–120.  
595 <https://doi.org/10.1016/j.icarus.2018.04.016>
- 596 Leonard, E. J., Yin, A., & Pappalardo, R. T. (2020). Ridged plains on Europa reveal a  
597 compressive past. *Icarus*, *343*, 113709. <https://doi.org/10.1016/j.icarus.2020.113709>
- 598 Lesage, E., Schmidt, F., Andrieu, F., & Massol, H. (2021). Constraints on effusive cryovolcanic  
599 eruptions on Europa using topography obtained from Galileo images. *Icarus*, *361*, 114373.  
600 <https://doi.org/10.1016/j.icarus.2021.114373>
- 601 Ligier, N., Poulet, F., Carter, J., Brunetto, R., & Gourgeot, F. (2016). Vlt/Sinfoni Observations of  
602 Europa: New Insights Into the Surface Composition. *The Astronomical Journal*, *151*(6),  
603 163. <https://doi.org/10.3847/0004-6256/151/6/163>
- 604 Manga, M., & Michaut, C. (2017). Formation of lenticulae on Europa by saucer-shaped sills.  
605 *Icarus*, *286*, 261–269. <https://doi.org/10.1016/j.icarus.2016.10.009>
- 606 Matteoni, P. (2022). Replication Data for: Ménéce Fossae on Europa: a Strike-Slip Tectonics  
607 Origin above a possible Shallow Water Reservoir. TRR170-DB.  
608 <https://doi.org/10.35003/8CU23S>
- 609 Matteoni, P., Mitri, G., Poggiali, V., & Mastrogiuseppe, M. (2020). Geomorphological Analysis  
610 of the Southwestern Margin of Xanadu, Titan: Insights on Tectonics. *Journal of*  
611 *Geophysical Research: Planets*, *125*(12), 1–22. <https://doi.org/10.1029/2020JE006407>
- 612 McCord, T. B., Hansen, G. B., Matson, D. L., Johnson, T. V., Crowley, J. K., Fanale, F. P., et al.  
613 (1999). Hydrated salt minerals on Europa's surface from the Galileo near-infrared mapping  
614 spectrometer (NIMS) investigation. *Journal of Geophysical Research: Planets*, *104*(E5),  
615 11827–11851. <https://doi.org/10.1029/1999JE900005>
- 616 Nimmo, F., & Pappalardo, R. T. (2016). Ocean worlds in the outer solar system. *Journal of*  
617 *Geophysical Research: Planets*, *121*(8), 1378–1399. <https://doi.org/10.1002/2016JE005081>
- 618 Nimmo, F., Pappalardo, R. T., & Giese, B. (2003). On the origins of band topography, Europa.  
619 *Icarus*, *166*(1), 21–32. <https://doi.org/10.1016/j.icarus.2003.08.002>
- 620 Nimmo, Francis, & Gaidos, E. (2002). Strike-slip motion and double ridge formation on Europa.  
621 *Journal of Geophysical Research*, *107*(E4), 5021. <https://doi.org/10.1029/2000JE001476>
- 622 Orlando, T. M., McCord, T. B., & Grieves, G. A. (2005). The chemical nature of Europa surface  
623 material and the relation to a subsurface ocean. *Icarus*, *177*(2), 528–533.  
624 <https://doi.org/10.1016/j.icarus.2005.05.009>
- 625 Pappalardo, R. T., Head, J. W., Greeley, R., Sullivan, R. J., Pilcher, C., Schubert, G., et al.  
626 (1998). Geological evidence for solid-state convection in Europa's ice shell. *Nature*,  
627 *391*(6665), 365–368. <https://doi.org/10.1038/34862>
- 628 Pappalardo, R. T., Belton, M. J. S., Breneman, H. H., Carr, M. H., Chapman, C. R., Collins, G.  
629 C., et al. (1999). Does Europa have a subsurface ocean? Evaluation of the geological  
630 evidence. *Journal of Geophysical Research: Planets*, *104*(E10), 24015–24055.  
631 <https://doi.org/10.1029/1998JE000628>
- 632 Petit, J. P. (1987). Criteria for the sense of movement on fault surfaces in brittle rocks. *Journal of*

- 633 *Structural Geology*, 9(5–6), 597–608. [https://doi.org/10.1016/0191-8141\(87\)90145-3](https://doi.org/10.1016/0191-8141(87)90145-3)
- 634 Postberg, F., Grün, E., Horanyi, M., Kempf, S., Krüger, H., Schmidt, J., et al. (2011).  
635 Compositional mapping of planetary moons by mass spectrometry of dust ejecta. *Planetary*  
636 *and Space Science*, 59(14), 1815–1825. <https://doi.org/10.1016/j.pss.2011.05.001>
- 637 Prockter, L. M., & Pappalardo, R. T. (2000). Folds on Europa: Implications for Crustal Cycling  
638 and Accommodation of Extension. *Science*, 289(5481), 941–943.  
639 <https://doi.org/10.1126/science.289.5481.941>
- 640 Prockter, L. M., Antman, A. M., Pappalardo, R. T., Head, J. W., & Collins, G. C. (1999).  
641 Europa: Stratigraphy and geological history of the anti-Jovian region from Galileo E14  
642 solid-state imaging data. *Journal of Geophysical Research: Planets*, 104(E7), 16531–  
643 16540. <https://doi.org/10.1029/1998JE001015>
- 644 Prockter, L. M., Head, J. W., Pappalardo, R. T., Sullivan, R. J., Clifton, A. E., Giese, B., et al.  
645 (2002). Morphology of European bands at high resolution: A mid-ocean ridge-type rift  
646 mechanism. *Journal of Geophysical Research*, 107(E5), 5028.  
647 <https://doi.org/10.1029/2000JE001458>
- 648 Quick, L. C., & Marsh, B. D. (2015). Constraining the thickness of Europa’s water–ice shell:  
649 Insights from tidal dissipation and conductive cooling. *Icarus*, 253, 16–24.  
650 <https://doi.org/10.1016/j.icarus.2015.02.016>
- 651 Rhoden, A. R., Mohr, K. J., Hurford, T. A., Henning, W., Sajous, S., Patthoff, D. A., & Dubois,  
652 D. (2021). Obliquity, Precession, and Fracture Mechanics: Implications of Europa’s Global  
653 Cycloid Population. *Journal of Geophysical Research: Planets*, 126(3).  
654 <https://doi.org/10.1029/2020JE006710>
- 655 Rossi, C., Cianfarra, P., Salvini, F., Mitri, G., & Massé, M. (2018). Evidence of transpressional  
656 tectonics on the Uruk Sulcus region, Ganymede. *Tectonophysics*, 749(March), 72–87.  
657 <https://doi.org/10.1016/j.tecto.2018.10.026>
- 658 Rossi, C., Cianfarra, P., Salvini, F., Bourgeois, O., & Tobie, G. (2020). Tectonics of Enceladus’  
659 South Pole: Block Rotation of the Tiger Stripes. *Journal of Geophysical Research: Planets*,  
660 125(12), 1–21. <https://doi.org/10.1029/2020JE006471>
- 661 Schenk, P., Matsuyama, I., & Nimmo, F. (2008). True polar wander on Europa from global-scale  
662 small-circle depressions. *Nature*, 453(7193), 368–371. <https://doi.org/10.1038/nature06911>
- 663 Schenk, P., Matsuyama, I., & Nimmo, F. (2020). A Very Young Age for True Polar Wander on  
664 Europa From Related Fracturing. *Geophysical Research Letters*, 47(17), 1–9.  
665 <https://doi.org/10.1029/2020GL088364>
- 666 Schenk, P. M., & Pappalardo, R. T. (2004). Topographic variations in chaos on Europa:  
667 Implications for diapiric formation. *Geophysical Research Letters*, 31(16), 1–5.  
668 <https://doi.org/10.1029/2004GL019978>
- 669 Schmidt, B. E., Blankenship, D. D., Patterson, G. W., & Schenk, P. M. (2011). Active formation  
670 of “chaos terrain” over shallow subsurface water on Europa. *Nature*, 479(7374), 502–505.  
671 <https://doi.org/10.1038/nature10608>
- 672 Schmidt, G., Luzzi, E., Rossi, A. P., Pondrelli, M., Apuzzo, A., & Salvini, F. (2022). Protracted  
673 Hydrogeological Activity in Arabia Terra, Mars: Evidence from the Structure and

- 674 Mineralogy of the Layered Deposits of Becquerel Crater. *Journal of Geophysical Research:*  
675 *Planets*. <https://doi.org/10.1029/2022JE007320>
- 676 Schubert, G., Sohl, F., & Hussmann, H. (2009). Interior of Europa. *Europa*, 353–367.
- 677 Singer, K. N., McKinnon, W. B., & Nowicki, L. T. (2013). Secondary craters from large impacts  
678 on Europa and Ganymede: Ejecta size–velocity distributions on icy worlds, and the scaling  
679 of ejected blocks. *Icarus*, 226(1), 865–884. <https://doi.org/10.1016/j.icarus.2013.06.034>
- 680 Sotin, C., Tobie, G., Wahr, J., McKinnon, W. B., McKinnon, W. B., & Khurana, K. K. (2009).  
681 Tides and tidal heating on Europa. *Europa*, 11.
- 682 Trumbo, S. K., Brown, M. E., Fischer, P. D., & Hand, K. P. (2017). A New Spectral Feature on  
683 the Trailing Hemisphere of Europa at 3.78  $\mu$  m. *The Astronomical Journal*, 153(6), 250.  
684 <https://doi.org/10.3847/1538-3881/aa6d80>
- 685 Trumbo, S. K., Brown, M. E., & Hand, K. P. (2019a). H<sub>2</sub>O<sub>2</sub> within Chaos Terrain on Europa's  
686 Leading Hemisphere. *The Astronomical Journal*, 158(3), 127. <https://doi.org/10.3847/1538-3881/ab380c>
- 687
- 688 Trumbo, S. K., Brown, M. E., & Hand, K. P. (2019b). Sodium chloride on the surface of Europa.  
689 *Science Advances*, 5(6), 2–6. <https://doi.org/10.1126/sciadv.aaw7123>
- 690 Trumbo, S. K., Becker, T. M., Brown, M. E., Denman, W. T. P., Molyneux, P., Hendrix, A., et  
691 al. (2022). A New UV Spectral Feature on Europa: Confirmation of NaCl in Leading-  
692 hemisphere Chaos Terrain. *The Planetary Science Journal*, 3(2), 27.  
693 <https://doi.org/10.3847/PSJ/ac4580>
- 694 Tufts, B. R., Greenberg, R., Hoppa, G., & Geissler, P. (1999). Astypalaea Linea: A Large-Scale  
695 Strike-Slip Fault on Europa. *Icarus*, 141(1), 53–64. <https://doi.org/10.1006/icar.1999.6168>
- 696 Vance, S., Harnmeijer, J., Kimura, J., Hussmann, H., DeMartin, B., & Brown, J. M. (2007).  
697 Hydrothermal Systems in Small Ocean Planets. *Astrobiology*, 7(6), 987–1005.  
698 <https://doi.org/10.1089/ast.2007.0075>
- 699 Vance, S. D., Hand, K. P., & Pappalardo, R. T. (2016). Geophysical controls of chemical  
700 disequilibria in Europa. *Geophysical Research Letters*, 43(10), 4871–4879.  
701 <https://doi.org/10.1002/2016GL068547>

702